ELSEVIER

Journal of Power Sources 84 (1999) 24–31

JOURNAL OF POWER SOURCES

www.elsevier.com/locate/jpowsour

Electrochemical characterization of various tin-based oxides as negative electrodes for rechargeable lithium batteries

S.C. Nam [a], C.H. Paik [b], W.I. Cho [b], B.W. Cho [b], H.S. Chun [a], K.S. Yun [b,*]

[a] *Department of Chemical Engineering, Korea University, Seoul 136-701, South Korea*

[b] *Battery and Fuel Cell Research Center, Korea Institute of Science and Technology, P.O. Box 131, Cheongryang, Seoul 130-650, South Korea*

Received 22 March 1999; accepted 5 April 1999

Abstract

Tin oxide and tin-based composite electrodes are examined in both bulk and thin-film form for prospective use as negative electrodes for lithium rechargeable batteries. For bulk electrodes, tin oxides and Sn–Zn–P–O composite materials are compared by charge–discharge testings. Thin films of oxides and composite thin-film electrodes prepared by heat treatment (temperature and time) are characterized by X-ray diffraction analysis, Auger electron spectroscopy, and scanning electron microscopy. The characteristics of thin films are found to depend on the heat-treatment temperature, which influences the structure, the grain size, and adhesion to the substrate. Capacities higher than 350 mA h g^{-1} are found for bulk electrodes beyond 20 cycles, and beyond 100 cycles for thin-film electrodes.

Keywords: Lithium rechargeable battery; Tin oxide; Tin-based composite; Negative electrode; Charge–discharge; Thin films

1. Introduction

Tin oxide and tin-based composite oxide electrodes have been considered [1–4] negative electrodes for lithium rechargeable batteries. Idota et al. [2] have found that Sn–B–Al–P–O amorphous composite oxides (TCO) exhibit high capacity performance. Using lithium-7 nuclear magnetic resonance measurements, they suggested that lithium was absorbed and stored in TCO in its ionic state. By using in-situ X-ray measurements, however, Courtney and Dahn [3] reported that SnO_2 irreversibly formed from Li_2O and metallic Sn, allows a reversible alloying reaction between Li and Sn [3]. They also studied [4] Sn_2BPO_6 glass and reported optimum cut-off voltage ranges for higher coulombic efficiencies, hence possibly extending cycle life beyond 100 cycles.

Bulk tin-based oxide and composite electrodes have been studied by other research groups who have found that the amorphous phase typically exhibits a high capacity. Liu et al. [5] prepared the oxides by precipitation methods to correlate cycle performance with heat-treatment conditions. Thin films of tin oxides show that oxides in crystalline form also display high capacities and long lives well beyond 100 cycles [6,7].

In this paper, the characteristics of tin oxide and tin-based composite electrodes in both bulk and thin-film form are compared. For bulk electrodes, the materials are prepared by thermal decomposition or synthesis. For a more fundamental study using a more homogeneous electrode surface, thin-film electrodes were prepared and studied. For thin films, a simple electron beam evaporation is used to deposit an oxide film from original tin oxide (SnO_2) and tin-based composite sources. The aim is to gain a better understanding of the influence of crystal structure and film morphology, controlled by heat-treatment conditions, on extending the cycle-life of these materials for high-capacity negative electrodes in lithium batteries.

2. Experimental

The preparation of tin oxide powders followed the method of Courtney and Dahn [4]. Tin (II) acetate was thermally decomposed in air at 420°C (sample A), and tin (IV) acetate (Aldrich) in argon at 390°C (sample B). Sn–Zn–P–O based composite glass was obtained from Mitsuya Boeki, and is designated as SEAN-31 (Seimi).

* Corresponding author. Tel.: +82-2-958-5221; fax: +82-2-958-5229; E-mail: ksyun@kistmail.kist.re.kr

0378-7753/99/$ - see front matter
PII: S0378-7753(99)00278-5

Inductively coupled plasma spectroscopy (ICP) and atomic adsorption spectroscopy (AAS) showed the composition to be $Sn_2Zn_{0.15}P_2O_{7.5}$. Bulk electrodes containing active material, were fabricated using polyvinylidene fluoride (PVDF, Kynar 761) binder and acetylene black conductor in NMP solvent on a copper grid (Delker) current-collector.

Thin film was deposited on a stainless-steel substrate from a pelletized tin oxide (Aldrich) or SEAN-31 powder (Seimi) source by e-beam evaporation apparatus (electron beam evaporation vacuum system (Leybold Univex 450)), an electron beam gun (Leybold ESV 6), and a deposition controller (Inficon IC-6000)). Film morphology and thickness were determined by scanning electron microscopy (SEM Hitachi S-4100), and the film weight was calculated from an assumed density of 6.99 g^{-3} cm^3 for SnO_2 [6] and 3.6 g^{-3} cm^3 for SEAN-31. The deposition ratio was 5 Å/s for SnO_2 and 10 Å/s for SEAN-31. The thin films were heat treated at 300, 400, 500 and 600°C in a furnace (Sybro 47900). The structure of the films treated at different temperatures were analyzed by X-ray diffraction analysis (XRD Rigaku). Auger electron spectroscopy (AES Perkin Elmer PHI-670) was used to determine the components and the depth profile of SEAN-31 thin film. The composition of the e-beam evaporated film from a SEAN-31 source was analyzed by ICP and Rutherford backscattering spectroscopy (RBS NEC, 6SPH2).

Cells were assembled with lithium foils (Cyprus) as counter and reference electrodes and 1 M $LiPF_6$ in EC:DMC (1:1) (thin film tin oxide), EC:DEC (1:1) (thin film SEAN-31) or PC:EC:DMC (1:1:3) (bulk electrodes) solvents (Merck). A polyethylene-based separator (Ube) was used. Constant-current galvanostatic charge–discharge tests were performed (Jisang JEC-180), and AC impedance analysis was obtained at different states of charge and discharge (Zahner, IM6).

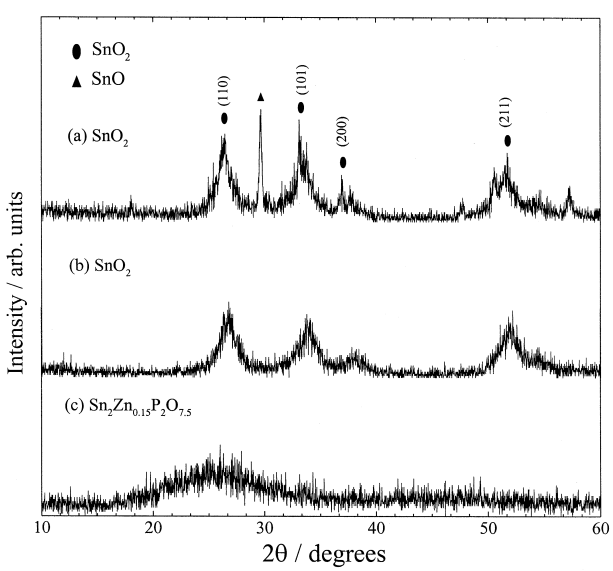

Fig. 1. X-ray diffraction patterns of: (a) tin oxide pyrolyzed from tin (II) acetate(air); (b) tin oxide pyrolyzed from tin (IV) acetate(argon); (c) Sn–Zn–P–O composite (SEAN-31, Seimi, Mitsuya Boeki).

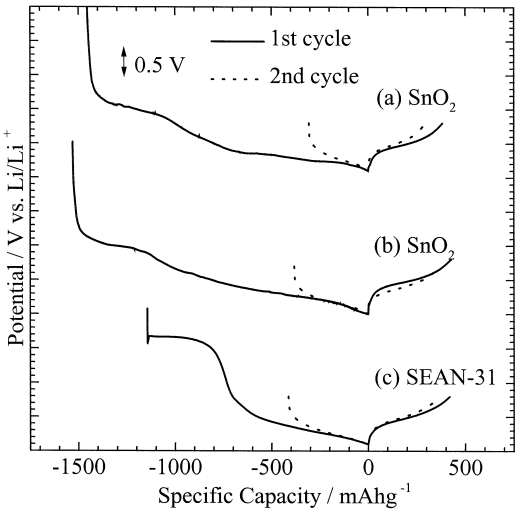

Fig. 2. Charge–discharge curves of: (a) tin oxide from tin (II) acetate; (b) tin oxide from tin (IV) oxide; (c) SEAN-31.

3. Results and discussion

3.1. Bulk electrode: tin oxides and tin-based composite SEAN-31

The X-ray diffraction patterns of tin oxide pyrolyzed from tin (II) acetate (sample A), tin oxide pyrolyzed from tin (IV) acetate (sample B), and (c) Sn–Zn–P–O composite (SEAN-31) are shown in Fig. 1. The XRD patterns for samples A and B resemble the samples obtained by Courtney and Dahn [4]: sample A showed the mixtures SnO as well as SnO_2. The grain size of SnO_2 (110) plane, calculated via the Scherrer equation [8], was 6.3 nm for sample A and 4.7 nm for sample B. The XRD patterns of SEAN-31 powders show virtually the same amorphous structure as the TCO composite [2]. It is assumed that this amorphous glass structure is similar to the weak diffraction pattern at $2\theta = 27$ to 28°, which is characteristic of SnO-containing glass and reflects a distribution of Sn–Sn distances in the anisotropic matrix, as reported by Idota et al. [2].

The charge–discharge characteristic curves of samples A, B, and SEAN-31 on the first and second cycles are presented in Fig. 2. The curves are composed of the initial side-reaction plateau (near 0.8 to 1.0 V vs. Li/Li^+ for tin oxides (A and B), and near 1.5 V for SEAN-31) and the broad lithium absorption plateau below 0.5 V vs. Li/Li^+. As expected, the side-reaction plateau was found to be independent of the type of electrolytic salt or solvent, but depended on the oxide content of the samples. The tin-based Sn–Zn–P–O composite shows a relatively low initial charge capacity, but a fast capacity recovery of about

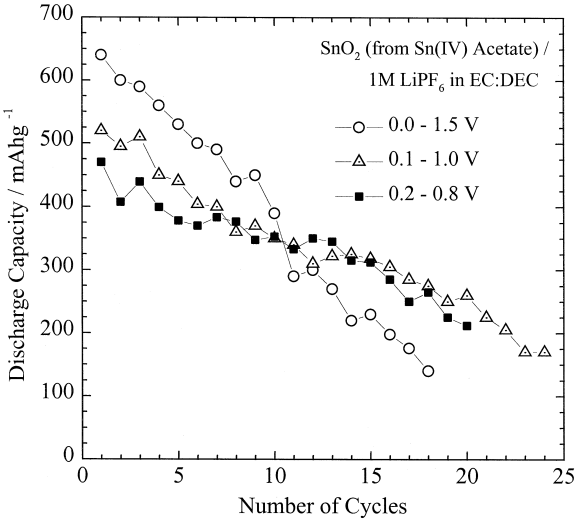

Fig. 3. Cycle performance of tin oxide pyrolyzed from tin (IV) acetate in 1 M $LiPF_6$ in EC:DEC (1:1).

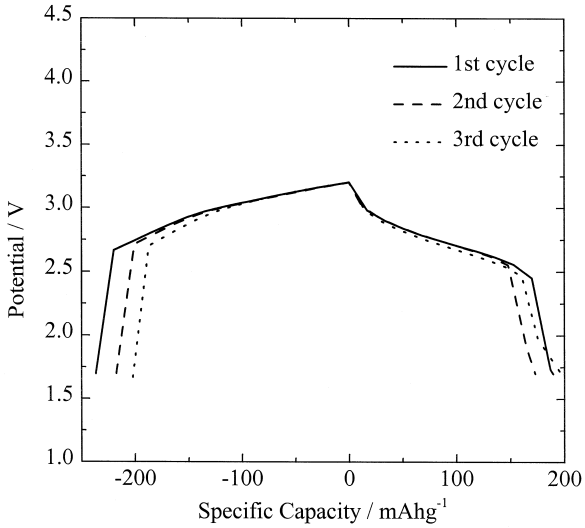

Fig. 4. Charge–discharge curve of lithiated SEAN-31/M1-PAN/V_6O_{13} cell.

413 mA h g^{-1} compared with other samples in the second charge.

The cycle performance of tin oxides (sample B) in 1 M $LiPF_6$ in EC:DEC(1:1) at three different cut-off voltages (0.0–1.5 V, 0.1–1.0 V and 0.2–0.8 V vs. Li/Li^+) are given in Fig. 3. When the voltage cut-off region is extended for further reaction with lithium (near 0.0 V vs. Li/Li^+), the lithium storage and discharge capacity are clearly extended. The efficiency (not included) was not, however, as high for the wide cut-off voltage, and hence, the capacity decayed down to about 150 mA h g^{-1} within 20 cycles. This means that the selection of an appropriate cut-off voltage range is important for the extension of cycle performance, as reported by Courtney and Dahn [4].

A preliminary charge–discharge characteristic curve for a lithiated SEAN-31/M1-PAN/V_6O_{13} cell at the C/5 rate is shown in Fig. 4. This cell involves a lithium ion polymer configuration, with a pre-lithiated SEAN-31 electrode coupled with a V_6O_{13} cathode material to accommodate the high capacity offered by SEAN-31. The active voltage was approximately 2.7–2.8 V and the capacity was about 200 mA h g^{-1}. The test lasted up to about 20 cycles.

3.2. Thin-film electrode

3.2.1. Tin oxides

Thin films of electron-beam deposited tin oxide are stable under atmospheric conditions and have good adhesion to the stainless-steel substrate. The X-ray diffraction patterns of e-beam deposited SnO_x films heat treated at 300, 400, 500 and 600°C for 4 h compared with an as-deposited film are given in Fig. 5. The original tin oxide source lost its highly crystalline structure during the physical vapour deposition process. The JCPDS reference (41–1445) confirmed the SnO_2 peaks at 26.61°, 33.89° and 37.95° which correspond to typical cassiterite structures. The main peak in this pattern, however, was (200) instead of the (110) cassiterite pattern. The broad peaks started to appear for a film heated to 400°C; the SnO (101) peak developed relatively stronger than the others. For a film heat treated at 600°C, the SnO_2 peaks, particularly (101) and (200), were developed strongly with the background peak from the stainless-steel substrate at 43.38 and 50.58°. Average grain size of the (200) plane annealed at 400 to about 600°C was 15 to about 50 nm, calculated by the Scherrer formula [8]. It is generally known that SnO_2 compounds evaporate into fragments, and result in an oxygen-deficient deposit consisting of SnO stoichiometry [9]. As-deposited amorphous SnO thin film was turned into crystalline SnO_2 by reaction with oxygen above 500°C. It

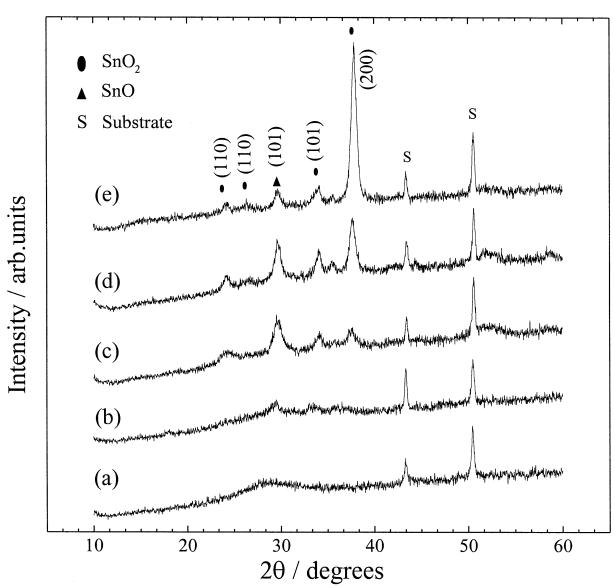

Fig. 5. X-ray diffraction patterns of (a) as-deposited film and films heat-treated at (b) 300°C, (c) 400°C, (d) 500°C, (e) 600°C for 4 h.

is suggested that the thin film that is annealed at 600°C consists mainly of SnO_2 with a slight amount of SnO. Poor adhesion and severe cracks between the thin film and substrate was observed when the thin film was annealed above 600°C; these are likely caused by thermal and mechanical stresses.

Scanning electron micrographs of the as-deposited and heat treated (600°C) SnO_2 thin films are given in Fig. 6. The as-deposited thin film showed an ill-defined, relatively featureless film. By contrast, the thin film which was heat treated at 600°C for 4 h showed a surface composed of a closed packed array of grains which were 20–60 nm wide. This value is very similar to that in Fig. 5 derived from the Scherrer formula. The actual crystalline structure was not observed at this magnification, but it is estimated that small crystallites are formed on the large grains during heat treatment.

The charge–discharge characteristic curves of electron beam deposited, thin film, tin oxide as deposited and after heat-treatment at 600°C are shown in Fig. 7. A reversible plateau is detected at 0.4 to 0.6 V. The irreversible plateau at 0.7 to 0.8 V is longer for the heat-treated film (740 mA h g^{-1}) than for the as-deposited film (490 mA h g^{-1}). The longer side-reaction plateau for the heat-treated film relates to the higher oxygen content as measured by the Auger depth profile. This behaviour has also been reported by Courtney and Dahn [3]. Using in situ XRD, these authors showed on initial charging the bulk SnO_2 was reduced to

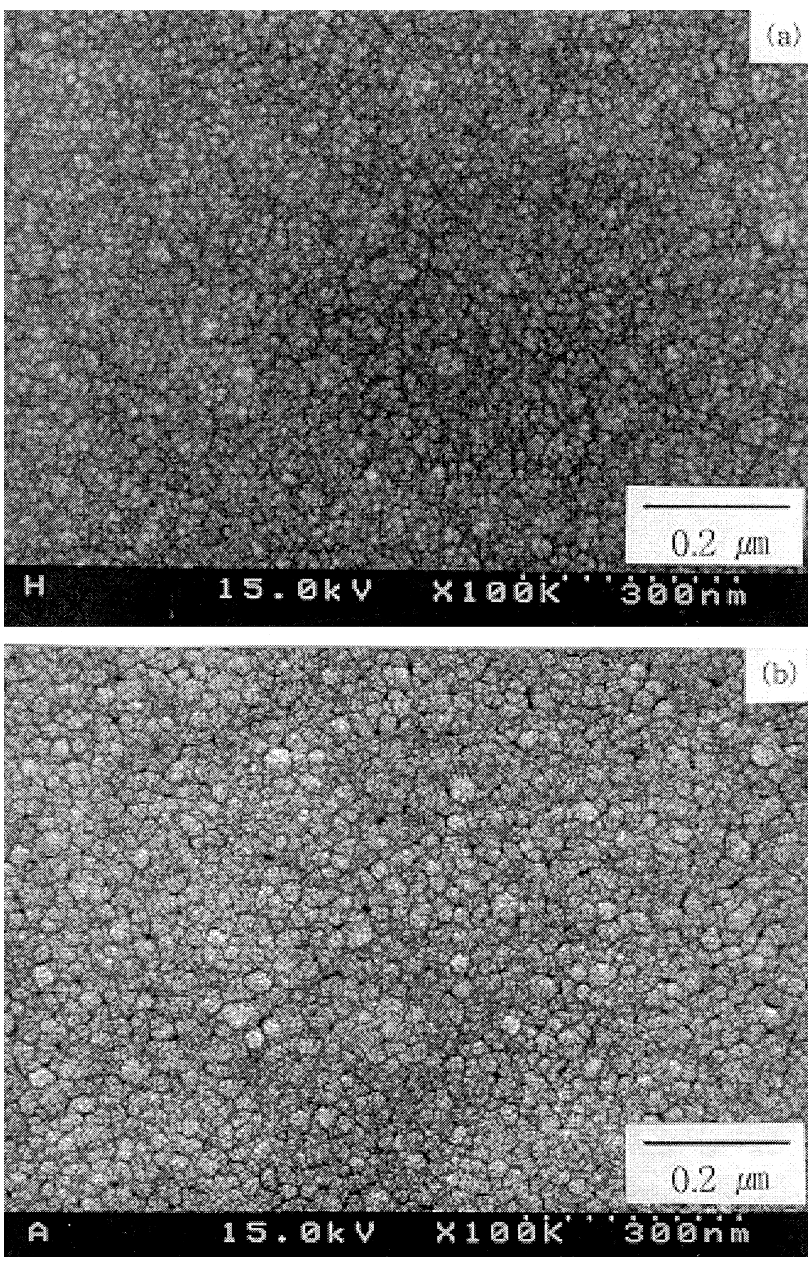

Fig. 6. Electron micrographs of (a) as-deposited film (b) and heat-treated (600°C) SnO_2 films.

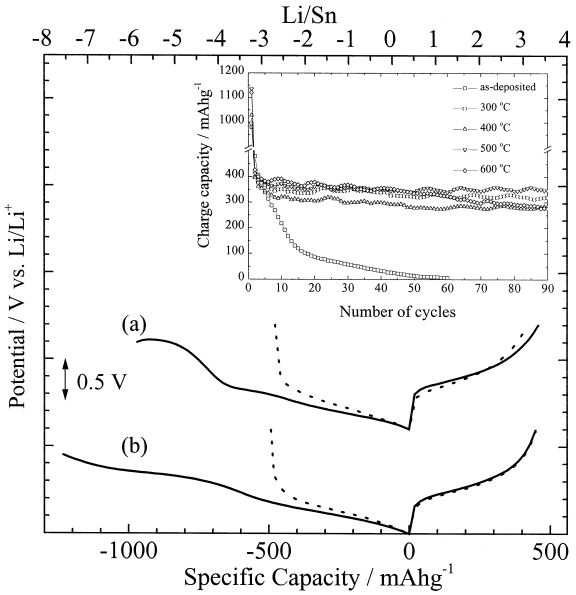

Fig. 7. Charge–discharge curves of electron beam deposited thin film tin oxide: (a) as deposited; (b) 600°C heat treated. Also, cycle performance of tin oxide films (1 μm thick) at various heat-treatment temperatures.

metallic Sn and amorphous $2Li_2O$ for the reaction of 4Li, and the Sn made an alloy of $Li_{4.4}Sn$ continuously by the reaction of 4.4Li. $Li_{4.4}Sn$, which was separated to metallic Sn and 4.4Li in the discharging state, was estimated to the reversible charge–discharge performance material for the lithium batteries. In this study, the Li:Sn mol. ratio has the very similar value to that suggested by Courtney and Dahn [3], but the reversible capacity, viz., $Li_{2.7}Sn$, was smaller. The cycle performance of tin oxide films (1 μm thickness) at various heat-treatment temperatures is also shown in Fig. 7. The data show that the as-deposited thin film decays in capacity to below 200 mA h g^{-1} within 10 cycles. Thin films treated at 300, 400, 500 and 600°C display similar cycle performance (about 300 mA h g^{-1} or higher) which persists for more than 100 cycles. If it is assumed that the metallic Sn, separated from tin oxide in the first charging state, is the reaction centre, the reason for capacity loss can be described as follows. First, adhesion to the substrate for the heat-treated film is stronger than that for the as-deposited film, which reduces the separation between the active material and the electrode caused by density differences between the materials formed by the charge–discharge reaction (SnO_2 6.9 g cm^{-3}, Li_2O 2 g cm^{-3}, Sn 7.3 g cm^{-3}, $Li_{22}Sn_5$ 2.6 g cm^{-3}). Actually, the degree of cracking of the as-deposited film surface after the first charging is more severe than that in the other heat-treated samples. Second, the as-deposited film contains an oxygen-deficient form of SnO, compared with the original SnO_2, which causes an insufficient Li_2O layer for reducing the degree of $Li_{22}Sn_5$ for an abrupt drop in capacity. Initial charge–discharge efficiency (beyond second cycle) is 95%, and rises above 97% after 20 cycles.

An AC impedance analysis of an annealed SnO_2 thin film (600°C, 4 h) during charging and discharging on the second cycle is presented in Fig. 8. The impedance values are adapted to a proposed equivalent circuit model which assumes a reaction centre of metallic tin surrounded by amorphous lithium oxide. The measured impedance values are matched with calculated values by complex nonlinear least-squares (CNLS) fitting. The simulated charge-transfer resistance decreases to 65 Ω when the electrode is charged to less than 0.2 V (vs. Li). But, when the cell is charged below 0.1 V (vs. Li), the charge-transfer impedance suddenly increases to about 278 Ω. This increase in impedance below 0.1 V (vs. Li) decreases again reversibly on discharge. It is speculated that such an increase in impedance is related to the lower coulombic efficiencies found for tin oxide anodes when the cut-off voltages are set below 0.2 V (vs. Li), as reported by Courtney and Dahn [4]. The increasing impedance behaviour may be related to a change in the Li–Sn phase, e.g., the formation of a $Li_{22}Sn_5$ phase, as reported by Brousse et al. [6].

An electron micrograph of the surface of an annealed SnO_2 thin film (600°C, 4 h) after the first cycle (C/5 rate) is shown in Fig. 9(a). There are microcracks of less than 1 μm in width. An as-deposited film contained severe cracks with little adhesion to the substrate compared with other heat-treated samples. Macroscopic cracks (−10 μm) were observed throughout the electrodes after 160 cycles (Fig. 9(b)]. Brusse et al. [6] attributed these cracks to density differences between the initial tin oxide film (6.9 g cm^{-3}) and Li_2O (2 g cm^{-3}), metallic Sn (7.3 g cm^{-3}), and alloys such as $Li_{22}Sn_5$ (2.6 g cm^{-3}).

3.2.2. Tin-based composite SEAN-31

The Auger spectrum of as-deposited SEAN-31 thin-film surface layer (thickness 0.9 μm) after 0.1 min sputtering is

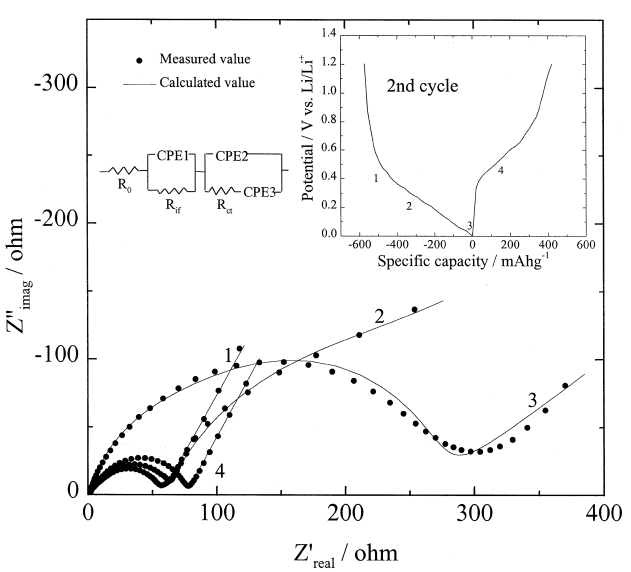

Fig. 8. AC impedance of heat-treated SnO_2 film during charging and discharging on second cycle.

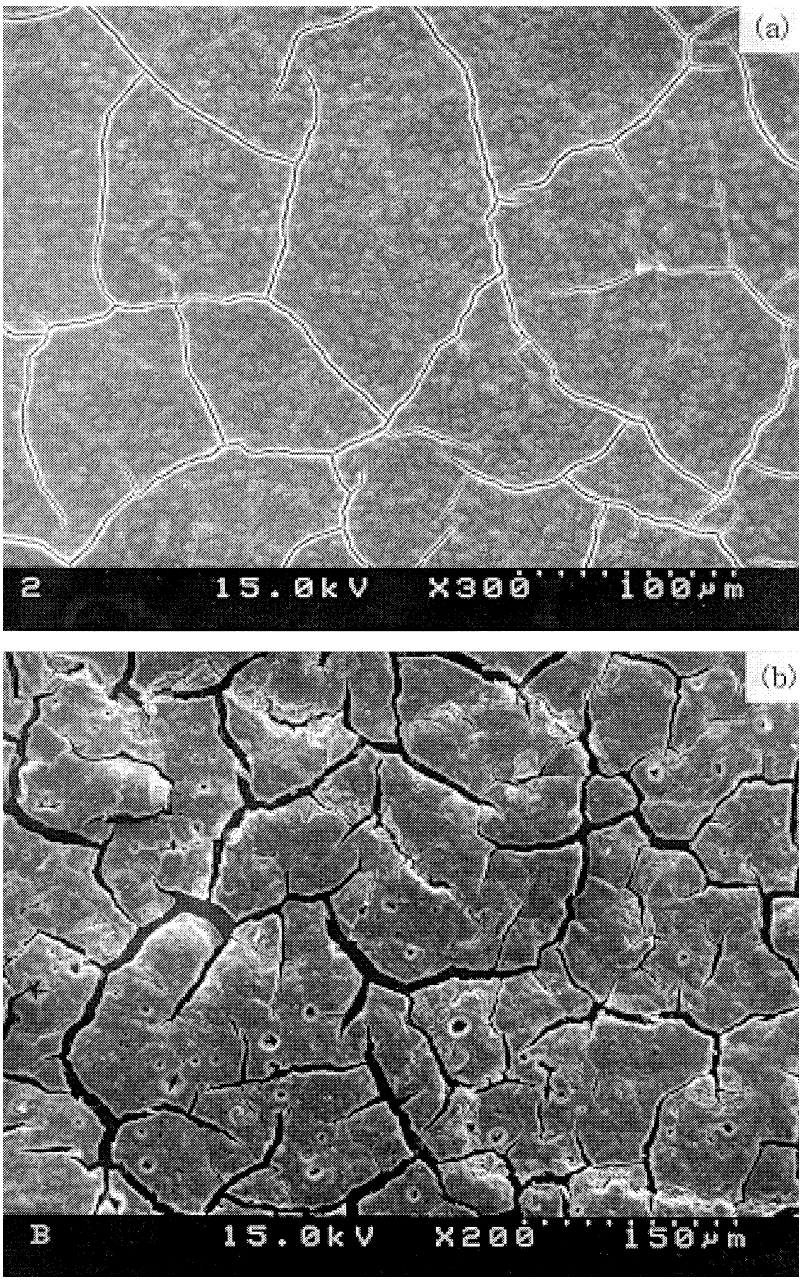

Fig. 9. Electron micrographs of surface of annealed (600°C, 4 h) film: (a) after first cycle; (b) after 160 cycles.

shown in Fig. 10(a). Qualitative analysis shows Sn, P, and O but no Zn compared to composition of $Sn_2Zn_{0.15}P_2O_{7.5}$ SEAN-31 powder. The trace amount of the Zn component may have been below the Auger's detection sensitivity. It is assumed that SEAN-31 source material evaporates into fragments like SnO_2 compounds, resulting in a Zn-free composition. ICP and RBS analysis reported a P:Sn ratio of 0.9 and a O:Sn ratio of 4.28, to give a $SnP_{0.9}O_{4.28}$ composition. Auger depth profile of the as-deposited film reveals that the components are grown homogeneously on to the stainless-steel substrate [Fig. 10(b)].

The charge–discharge curves of thin films electron beam deposited from a pelletized SEAN-31 source in (a) as deposited and (b) heat-treated forms are presented in Fig. 11. Both the as-deposited and heat-treated (400°C, 4 h) films undergo side reactions in near the 1.2 to 1.3 V region, then absorb lithium under 0.5 V vs. Li/Li^+. The heat-treated film showed a more stable side-reaction region, with a higher lithium absorption (charging) and extraction (discharging). The capacity of the as-deposited thin film declined drastically within ten cycles, but the heat-treated 0.9 μm SEAN-31 thin films have a much higher and more stable capacity cycle performance which was about 400 mA h g^{-1} after ten cycles. XRD analysis showed that the structures of the as-deposited film and films annealed up to 400°C are amorphous, but become crystalline after treatment at 500°C. The surface film heat treated at 400°C is heterogeneous, with random segrega-

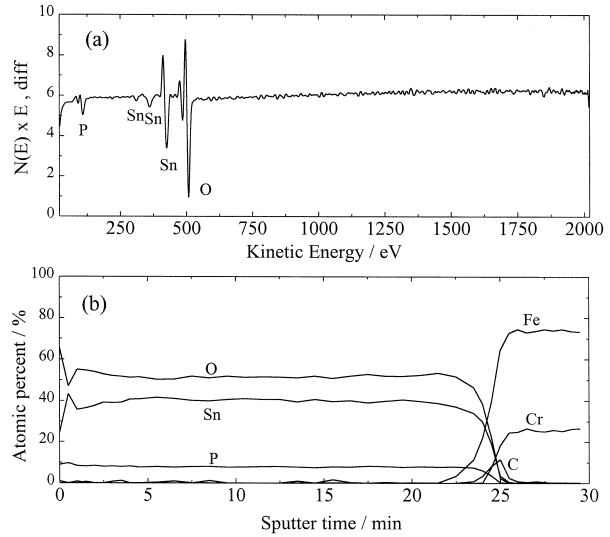

Fig. 10. (a) Auger spectrum and (b) depth profile of 0.9 μm thickness as-deposited SEAN-31 thin film surface layer after 0.1 min sputtering.

tions of 10 to 30 μm sized islands. Large craters of 30 μm are found in thin films annealed at 500°C. Electron probe microanalysis could not distinguish clearly the compositions of the various phase regions. Although it is not expected that there should be any effect on structural changes by heat treatment up to 400°C, since the material is already in an amorphous glassy state, the heat treatment in oxidizing conditions appears to influence the texture, the adhesion to substrate and the local mechanical stresses in the thin film. This appears to be unimportant for the thin-film structure given the fact that the crystalline SEAN-31 thin film annealed at 500°C also yields a high

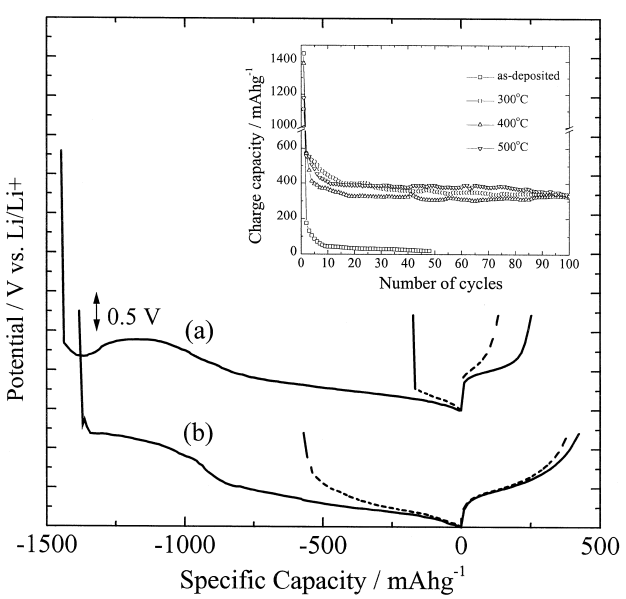

Fig. 11. Charge–discharge curves of thin films electron beam deposited from pelletized SEAN-31 source in (a) as deposited and (b) heat-treated form. Also, cycle performance at various heat-treatment temperatures.

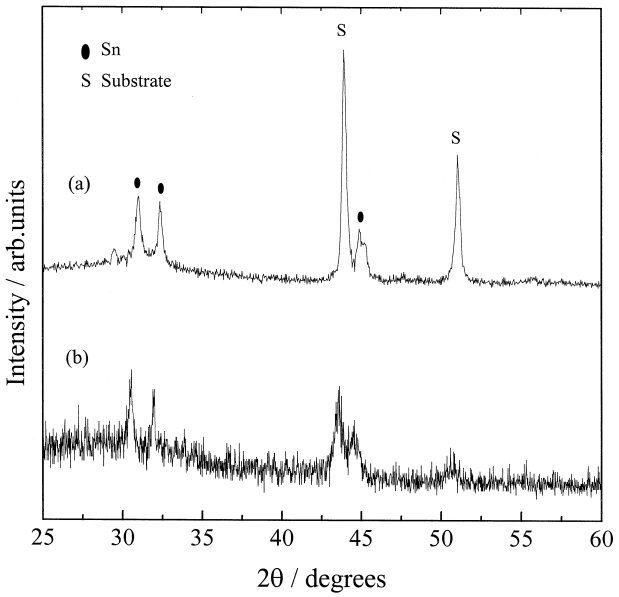

Fig. 12. X-ray diffraction patterns of e-beam deposited (a) tin oxide (500°C) and (b) SEAN-31 (500°C) films after 1st discharge (1.2 V vs. Li/Li^+).

capacity. The reason for the higher capacity performance when the thin film is heat treated, is still not fully understood.

The X-ray diffraction patterns of e-beam deposited (a) tin oxide (500°C) and (b) SEAN-31 (500°C) films after the

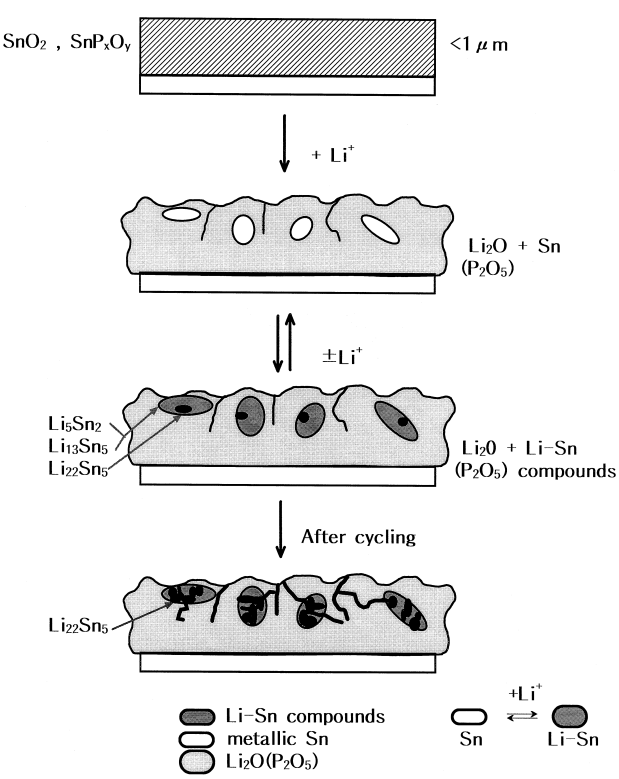

Fig. 13. Proposed mechanism of lithium interaction with thin tin oxide and composite films.

first discharge (1.2 V vs. Li/Li^+) are shown in Fig. 12. The data support the results reported by Courtney and Dahn [3] for the metallic tin peaks at 30.57, 32.06 and 44.57°. It is understood that the structure of the initial tin oxide or the tin-based composite oxide is transformed on the first cycle, and metallic tin may be a reaction centre with lithium in further cycles.

The proposed mechanism of lithium interaction with the thin tin oxide and composite films is summarized in Fig. 13. Thin films with thicknesses of 1 μm or less react with lithium on the first charge are reduced to $Li_2O(P_2O_5)$ and metallic Sn due to an irreversible side reaction. Tin continuously forms Li–Sn compounds such as Li_5Sn_2, $Li_{13}Sn_5$, $Li_{22}Sn_5$ on reaction with lithium and a reversible reaction is generated between Sn and the Li–Sn compounds. Microcracks are formed because of density differences and the cycle life is decreased as a result of irreversible $Li_{22}Sn_5$ formation with cycling. Annealed SEAN-31 thin films (SnP_xO_y compounds) display high capacity and good cycling behaviour compared with tin oxide films. Thus, it is suggested that the network structures between P_2O_5 and Li_2O matrix are advantageous in an anode system, but it is not yet understood what effects are exerted on the cycling behaviour of P_2O_5.

4. Conclusions

Bulk and thin film electrodes of tin oxide and composite have been examined. The electrodes show little dependence on the type of electrolytic solution, but rather strong dependence on the initial structure in terms of charge–discharge performance. The cut-off voltages influence the reversibility of alloying phases between lithium and metallic tin. Preliminary tests of a negative electrode consisting of SEAN-31 active material are reported. A bulk system yields a capacity of 300 to 400 mA h g^{-1} which lasts up to 20 cycles with proper control of the cut-off voltage. The Sn-based glass material is a promising negative electrode for lithium polymer rechargeable batteries. The morphology and structure of an electron beam evaporated tin oxide film have been examined. The effects of heat treatment, film thickness and kinetic rates are evaluated by constant current charge–discharge testing. Heat treatment results in more defined grain structures (small crystallites with a large grain size) and higher performance in capacity and cycle life with homogeneous composition. Rapid loss in capacity is attributed to poor film adhesion with the substrate rather than to an amorphous or crystalline structure. Microcracks formed during cycling also influence the capacity loss. Impedance measurements suggest that the alloying reaction between lithium and metallic tin causes a decrease in the charge-transfer resistance down to a certain critical state-of-charge, beyond which the resistance increases again. AES, ICP and RBS analysis of thin film SEAN-31 systems suggest a possible change in the stoichiometry of the bulk powder. Despite non-uniformity and heterogeneity, a heat-treated electrode exhibits higher capacity (400 mA h g^{-1}) and more stable cycle performance. Electron beam deposited thin films from pelletized SEAN-31 are possible candidates for thin film batteries.

References

[1] Y. Idota, M. Mishima, M. Miyaki, T. Kubota, T. Miyasaka, Eur. Pat. Appl. 651450 Al 950503.
[2] Y. Idota, A. Matsufuji, Y. Maekawa, T. Miyasaki, Science 276 (1997) 1395.
[3] I.A. Courtney, J.R. Dahn, J. Electrochem. Soc. 144 (1997) 2045.
[4] I.A. Courtney, J.R. Dahn, J. Electrochem. Soc. 144 (1997) 2943.
[5] W. Liu, X. Huang, Z. Wang, H. Li, L. Chen, J. Electrochem. Soc. 145 (1998) 59.
[6] T. Brousse, R. Retoux, U. Herterich, D.M. Schleich, J. Electrochem. Soc. 145 (1998) 1.
[7] S.C. Nam et al., Electrochemical and Solid-State Letters 2 (1999) 9.
[8] B.D. Cullity, Elements of X-ray Diffraction, 2nd edn., Addison-Wesley, MA, 1978, p. 102.
[9] Bunshah, Deposition Technologies for Films and Coatings, Noyes Publications, Park Ridge, NJ, 1982, p. 124.